THE JOURNAL OF BIOLOGICAL CHEMISTRY VOL. 285, NO. 45, pp. 35011–35020, November 5, 2010

Cysteine-scanning Analysis of Helices TM8, TM9a, and TM9b and Intervening Loops in the YgfO Xanthine Permease

A CARBOXYL GROUP IS ESSENTIAL AT ASP-276[*][S]

Received for publication, July 30, 2010, and in revised form, August 27, 2010 Published, JBC Papers in Press, August 29, 2010, DOI 10.1074/jbc.M110.170415

George Mermelekas, Ekaterini Georgopoulou, Alexander Kallis, Maria Botou, Vassilios Vlantos, and Stathis Frillingos[1]
From the Laboratory of Biological Chemistry, University of Ioannina Medical School, 45110 Ioannina, Greece

Bacterial and fungal members of the ubiquitous nucleobase-ascorbate transporter (NAT/NCS2) family use the NAT signature motif, a conserved 11-amino acid sequence between amphipathic helices TM9a and TM9b, to define function and selectivity of the purine binding site. To examine the role of flanking helices TM9a, TM9b, and TM8, we employed Cys-scanning analysis of the xanthine-specific homolog YgfO from *Escherichia coli*. Using a functional mutant devoid of Cys residues (C-less), each amino acid residue in sequences ^{259}FLVVGTIYLLSVLEAVGDITATAMVSRRPIQGEEYQSRLKGGVLADGLVSVIASAV^{314} and ^{342}TIAVMLVILGLFP^{354} including these TMs (underlined) was replaced individually with Cys, except the irreplaceable Glu-272 and Asp-304, which had been studied previously. Of 67 single Cys mutants, 55 accumulate xanthine to 35–140% of the steady state observed with C-less, five (I265C, D276C, I277C, G299C, L350C) accumulate to low levels (10–20%) and seven (T278C, A279C, T280C, A281C, G305C, G351C, P354C) show negligible expression in the membrane. Extensive mutagenesis reveals that a carboxyl group is needed at Asp-276 for high activity and that D276E differs from wild type as it recognizes 8-methylxanthine (K_i 79 μM) but fails to recognize 2-thioxanthine, 3-methylxanthine or 6-thioxanthine; bulky replacements of Ala-279 or Thr-280 and replacements of Gly-305, Gly-351, or Pro-354 impair activity or expression. Single Cys mutants V261C, A273C, G275C, and S284C are sensitive to inactivation by *N*-ethylmaleimide and sensitivity of G275C (IC_{50} 15 μM) is enhanced in the presence of substrate. The data suggest that residues crucial for the transport mechanism cluster in two conserved motifs, at the cytoplasmic end of TM8 (E*XX*G-D*XX*AT) and in TM9a (G*XXX*DG).

The nucleobase-ascorbate transporter (NAT)[2] or nucleobase-cation symporter-2 (NCS2) family is an evolutionarily ubiquitous family of purine, pyrimidine, and L-ascorbate transporters, with members specific for cellular uptake of uracil, xanthine, or uric acid (microbial, plant and non-primate mammalian genomes) or vitamin C (mammalian genomes) (1–3). Despite their importance for the recognition and uptake of several frontline purine-related drugs, NAT/NCS2 members have not been studied systematically at the molecular level and high-resolution structures or mechanistic models are missing. More than 1,000 sequence entries are known but few are functionally characterized to date. Structure-function relationships have been studied extensively in two members, the eukaryotic UapA, a high-affinity uric acid/xanthine:H^+ symporter from the ascomycote *Aspergillus nidulans* (3–6) and the prokaryotic YgfO, a specific, high-affinity xanthine:H^+ symporter from *Escherichia coli* (7–11). Mutagenesis data from both lines of study have shown that key NAT determinants are strikingly similar between the two transporters, and that few residues conserved throughout the family may be invariably critical for function (10).

Of more than 160 residues of YgfO permease studied thus far with site-directed mutagenesis (8–11), four have been delineated as functionally irreplaceable (Glu-272, Asp-304, Gln-324, Asn-325) (Fig. 1).[3] Of them, Asn-325 and Gln-324 belong to the NAT signature motif, a conserved 11-amino acid sequence between amphipathic helices TM9a and TM9b, and site-directed alkylation analysis suggests that they participate directly in the substrate binding site (11). The other two irreplaceable residues of YgfO are in the neighboring helices TM8 (Glu-272) and TM9a (Asp-304) and appear to be implicated with the conformational changes following binding and/or coupling purine with proton translocation, but not with substrate binding *per se* (10). Apart from the irreplaceable ones, a number of other important residues have been found, including residues at the middle of helices TM1 (His-31) and TM3 (Asn-93), which contribute to determining the proper affinity and selectivity of the purine binding site (10), residues at the middle of TM12 (Asn-430, Ile-432), which are close to the binding site and/or optimize binding indirectly (9), and residues within or adjacent to the NAT motif which are important conformationally (Ala-323) (11) or involved in defining the optimal specificity profile (Thr-332, Gly-333, Ser-336) (8, 11). Overall, residues delineated as crucial for the mechanism of substrate recognition and selectivity cluster primarily at the NAT motif region (Fig. 1). Similar crucial roles have been reported for corresponding con-

* This work is part of the 03ED204 research project, implemented within the framework of the "Reinforcement Programme of Human Research Manpower" (PENED) and co-financed by National and Community Funds (25% from the Greek Ministry of Development, General Secretariat for Research and Technology, and 75% from the European Union European Social Fund).
[S] The on-line version of this article (available at http://www.jbc.org) contains supplemental Figs. S1 and S2 and Table S1.
[1] To whom correspondence should be addressed: University of Ioannina Medical School, Laboratory of Biological Chemistry, 45110 Ioannina, Greece. E-mail: efriligo@cc.uoi.gr.
[2] The abbreviations used are: NAT, nucleobase-ascorbate transporter; TM, transmembrane helix; NEM, *N*-ethylmaleimide; IPTG, isopropyl 1-thio-β-D-galactopyranoside; BAD, biotin-acceptor domain; Cys-less (C-less), permease devoid of native Cys residues; PMS, phenazine methosulfate.
[3] G. Mermelekas and S. Frillingos, manuscript in preparation.

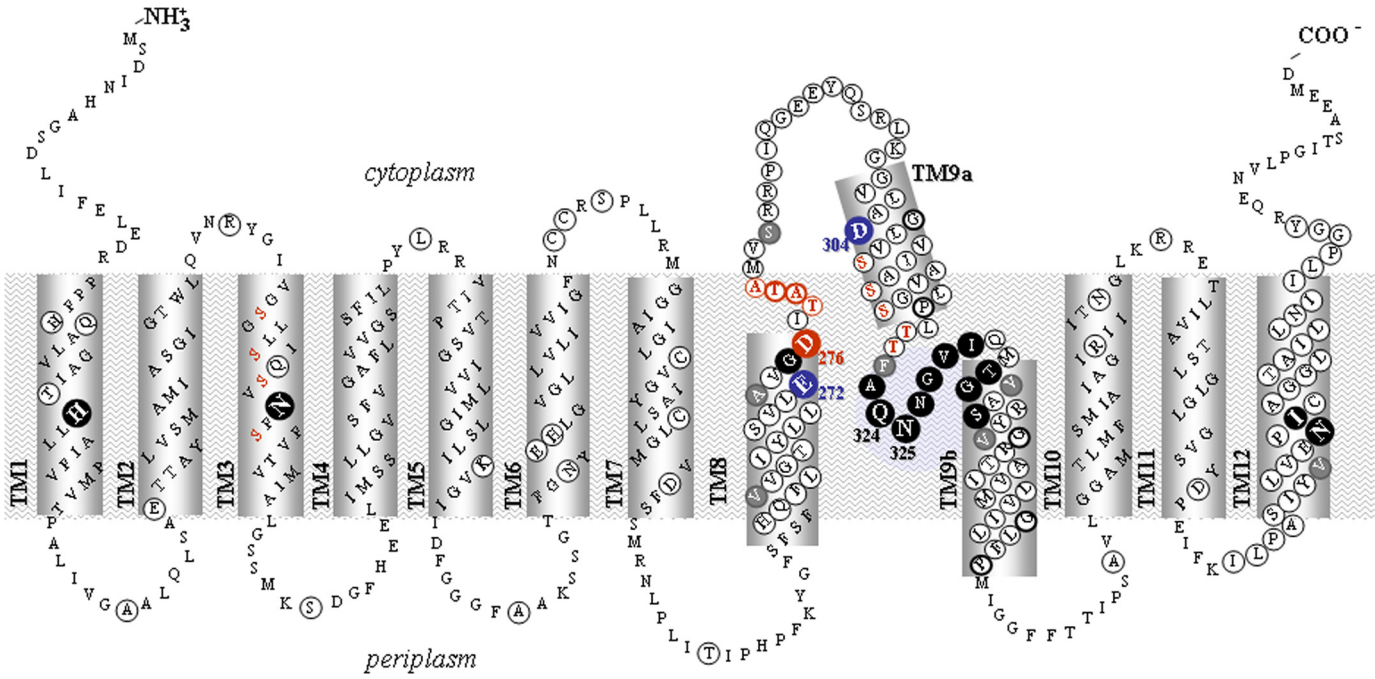

FIGURE 1. **Topology model of YgfO permease.** The model is based on program TMHMM, evidence that C terminus is cytoplasmic (7, 15) and our unpublished evidence (see footnote 3) on the accessibility of loops to hydrophilic reagents. Irreplaceable residues of YgfO (10) are *numbered and bolded*. NEM-sensitive positions are shown in *dark background*. Residues analyzed with site-directed mutagenesis are *circled*. The ambiguous topology segment 299–319 upstream of the NAT motif is designated as TM9a, and the amphipathic segment 330–354 that follows is designated as TM9b. The short intervening sequence between TM9a and TM9b is shown as a re-entrant loop facing the internal hydrophilic cavity, based on our evidence on the solvent accessibility and the substrate recognition properties of residues of the NAT motif (11). Residue Asp-276 (TM8) and the downstream sequence ^{278}TATA^{281} delineated as important in this study as well as residues forming a contiguous α-helical hydrophilic face in TM9a are shown *in red*.

served residues of the NAT motif in the fungal homolog UapA (4, 5).

Recently, Cys-scanning and substituted-Cys accessibility analysis (11) has shown that the NAT motif of YgfO permease may form a re-entrant loop between helices TM9a and TM9b that faces the central hydrophilic cavity and is accessible to substrate and solvent from the periplasmic side (Fig. 1). This arrangement brings putative transmembrane helix TM8 in closer proximity with the NAT motif or the flanking helices TM9a and TM9b than it could be predicted from topology algorithms (4, 10–12) and implies that these helices may contain additional important determinants for the mechanism of substrate recognition and uptake. In this report, employing systematic site-directed mutagenesis in the YgfO sequence 259–354 (Fig. 1) and analysis of a set of 109 engineered mutants (supplemental Table S1), we show that residues important for function or expression in the membrane cluster in two additional conserved sequence motifs, one at the end of TM8 (**E***XX***G**D*XX***A**T) and one in TM9a (G*XXX***DG**), as well as in motif G*XX*P at the end of TM9b (supplemental Fig. S1). These residues include the functionally irreplaceable Glu-272 (TM8) and Asp-304 (TM9a) identified previously (10), Asp-276, where a carboxyl group is needed for high activity, Gly-275, where site-specific alkylation of an engineered Cys abolishes transport, Ala-279 and Thr-280, where bulkier side chains impair activity, Gly-305, Gly-351, and Pro-354, where replacements lead to low activity or impaired expression in the membrane. Three of these residues (Glu-272, Gly-275, and Asp-276 in motif **E***XX***G**D*XX***A**T) form an α-helical face at the cytoplasmic end of TM8, which emerges as crucial for the transport mechanism.

EXPERIMENTAL PROCEDURES

Materials—[8-^{3}H]xanthine (27.6 Ci mmol^{-1}) and [8-^{14}C]uric acid (51.5 mCi mmol^{-1}) were purchased from Moravek Biochemicals. Non-radioactive nucleobases and analogues were from Sigma. Oligodeoxynucleotides were synthesized from BioSpring GmbH. High fidelity Taq Polymerase (Phusion High Fidelity PCR System) was from Finnzymes. Restriction endonucleases used were from Takara. *N*-Ethylmaleimide (NEM) was from Sigma. Horseradish peroxidase (HRP)-conjugated avidin was from Amersham Biosciences. All other materials were reagent grade and obtained from commercial sources.

Bacterial Strains and Plasmids—*E. coli* K-12 was transformed according to Inoue (13). TOP10F' (Invitrogen) was used for initial propagation of recombinant plasmids. T184 (14) harboring pT7-5/*ygfO* (7) with given replacements was used for IPTG-inducible expression from the *lacZ* promoter/operator.

DNA Manipulations—Construction of expression plasmids and BAD (biotin-acceptor domain)-tagged versions of YgfO has been described (7). For construction of Cys-less YgfO, the five native Cys codons were replaced simultaneously with Ser codons, using two-stage (multiple overlap/extension) PCR on the template of wild-type YgfO tagged at C terminus with the BAD tag (8). For construction of mutants, two-stage PCR was performed on the template of Cys-less or wild-type YgfO, as indicated. The entire coding sequence of all engineered constructs was verified by double-strand DNA sequencing in an

automated DNA sequencer (MWG-Biotech) (supplemental Table S1).

Growth of Bacteria—Escherichia coli T184 harboring given plasmids was grown aerobically at 37 °C in Luria-Bertani medium containing streptomycin (0.01 mg/ml) and ampicillin (0.1 mg/ml). Fully grown cultures were diluted 10-fold, allowed to grow to mid-logarithmic phase, induced with IPTG (0.5 mM) for an additional 2 h at 37 °C, harvested, and washed with appropriate buffers.

Transport Assays and Kinetic Analysis—E. coli T184 were assayed for active transport of [^{3}H]xanthine (1 μM), by rapid filtration, at 25 °C, pH 7.5, as described (7). For kinetic uptake measurements, initial rates were assayed in T184 cells, at 5–20 s, in the concentration range of 0.1–100 μM [^{3}H]xanthine. Selected mutants were also assayed for transport of [^{14}C]uric acid (0.04–2 mM), using the paralog YgfU as a positive control.[4] For assaying the effect of NEM on xanthine uptake activity, T184 cells were preincubated with NEM at the indicated conditions, excess reagents and ligands were removed by centrifugation, and transport assays were performed in the presence of phenazine methosulfate (PMS) (0.2 mM) and potassium ascorbate (20 mM) (8). For ligand competition experiments, uptake of [^{3}H]xanthine (1 μM) was assayed in the absence or presence of unlabeled analogues (1 mM) (7). For kinetic analysis, putative inhibitors were used in the concentration range of 1 μM to 2 mM, and data were fitted to the equation $y = B + (T - B)/(1 + 10^{((\log IC_{50} - \log x)\, h)})$ for sigmoidal dose-response (variable slope), where x is the concentration variable, y (activity) values range from T (*top*) to B (*bottom*) and h is the Hill coefficient, for sigmoidal dose-response (variable slope), using Prism4, to obtain IC_{50} values; in all cases, the Hill coefficient was close to −1, consistent with presence of one binding site. K_i values for each analog were calculated from the Cheng and Prusoff equation $K_i = IC_{50}/[1 + (L/K_m)]$ (where L is the permeant concentration and K_m is the value obtained for this permeant), assuming a simple model of competitive inhibition with the binding site of the transporter (8); competitive inhibition has been shown with certain analogues (1-methyl, 2-thio, and 8-methylxanthine) by assaying their effect on K_m and V_{max} for wild type and selected mutants, and showing that V_{max} remains unaltered (8–10).

Immunoblot Analysis—Membrane fractions were prepared from 10-ml cultures of *E. coli* T184 harboring given plasmids and subjected to SDS-PAGE (12%), as described (7). Proteins were electroblotted to poly(vinylidene difluoride) membranes (Immobilon-PVDF; Pall Corp.). YgfO-BAD was probed with avidin-HRP. Signals were developed with enhanced chemiluminescence (ECL).

In Silico Analysis—Comparative sequence analysis of NAT/NCS2 homologs was based on BLAST-p search and ClustalW alignment; the most recent genome annotations were used for retrieving sequence data. Initial analysis of transmembrane topology was performed using program TMHMM (15).

[4] K. Papakostas and S. Frillingos, manuscript in preparation.

RESULTS

Active Xanthine Transport—Using a functional YgfO permease devoid of Cys residues (C-less), each amino acid residue in sequences ^{259}FLVVGTIYLLSVLEAVGDITATAMVSRRPIQGEEYQSRLKGGVLADGLVSVIASAV^{314} and ^{342}TIAVMLVILGLFP^{354} including putative amphipathic helices TM8, TM9a, and TM9b (underlined) was replaced individually with Cys, except Glu-272 and Asp-304, which had been studied by us previously (10). After verification of the sequence, each single Cys mutant was transformed into *E. coli* T184 and assayed for its ability to catalyze active xanthine transport. As shown in Fig. 2*A*, of the 67 single Cys mutants, 54 transport xanthine at rates between 40 and 170% of C-less permease, two (V261C, I265C) transport at lower rates (20–25%), four (D276C, I277C, G299C, L350C) display very low but detectable rates (5–10%) and seven (T278C, A279C, T280C, A281C, G305C, G351C, P354C) display rates that are indistinguishable from cells containing no *ygfO* insert. Steady state levels of xanthine accumulation also show the same general picture (Fig. 2*B*); of the 67 single Cys mutants, 55 accumulate xanthine to 35–140% of the steady state observed with C-less YgfO, five (I265C, D276C, I277C, G299C, L350C) accumulate to low levels (10–20%), and seven (T278C, A279C, T280C, A281C, G305C, G351C, P354C) are inactive.

Expression in the Membrane—Immunoblot analysis of BAD-tagged single Cys permeases shows that negligible activity of mutants T278C, A279C, T280C, A281C, G305C, G351C, and P354C is associated with negligible expression in the membrane. All other mutants are expressed to high or moderate levels comparable with those of C-less YgfO (Fig. 3). The compromised expression (~25% of C-less) displayed by mutant I277C reflects its low transport rate (10% of C-less) (Fig. 2).

Expression and Transport Analysis of Mutants in Wild Type Background—From the Cys-scanning transport analysis described above, 11 positions of inactive or low activity mutants were delineated. We analyzed these positions further by (*a*) transferring single Cys mutations to the wild-type YgfO background and/or (*b*) engineering the most conservative site-directed replacement mutants to introduce an amino acid other than Cys. For positions of aliphatic native residues (Ile-277, Leu-350), we constructed and assayed mutants I277L(wt), L350V(wt), and L350I(wt), which exhibited approximately wild-type levels of expression and xanthine uptake activity (Fig. 4). For positions of a native Gly or Pro (Gly-299, Gly-305, Gly-351, Pro-354), we constructed and analyzed mutants G299C(wt), G305C(wt), G305A(wt), G305P(wt), G351A(wt), G351P(wt) and P354G(wt); of them, G299C(wt) displays wild-type levels of expression and activity, G305A(wt), G351A(wt), and P354G(wt) are expressed to high levels but yield low activity (xanthine uptake rates and levels of 20–40% relative to wild type), and G305C(wt), G305P(wt), and G351P(wt) show negligible or marginal expression in the membrane and are inactive (Fig. 4). For the remaining 5 positions (Fig. 2), we performed a more extensive mutagenesis study, as described below (Figs. 5 and 6 and Table 1).

Replacements of Asp-276—We constructed and analyzed 10 different side-chain replacement mutants of YgfO(wt) at posi-

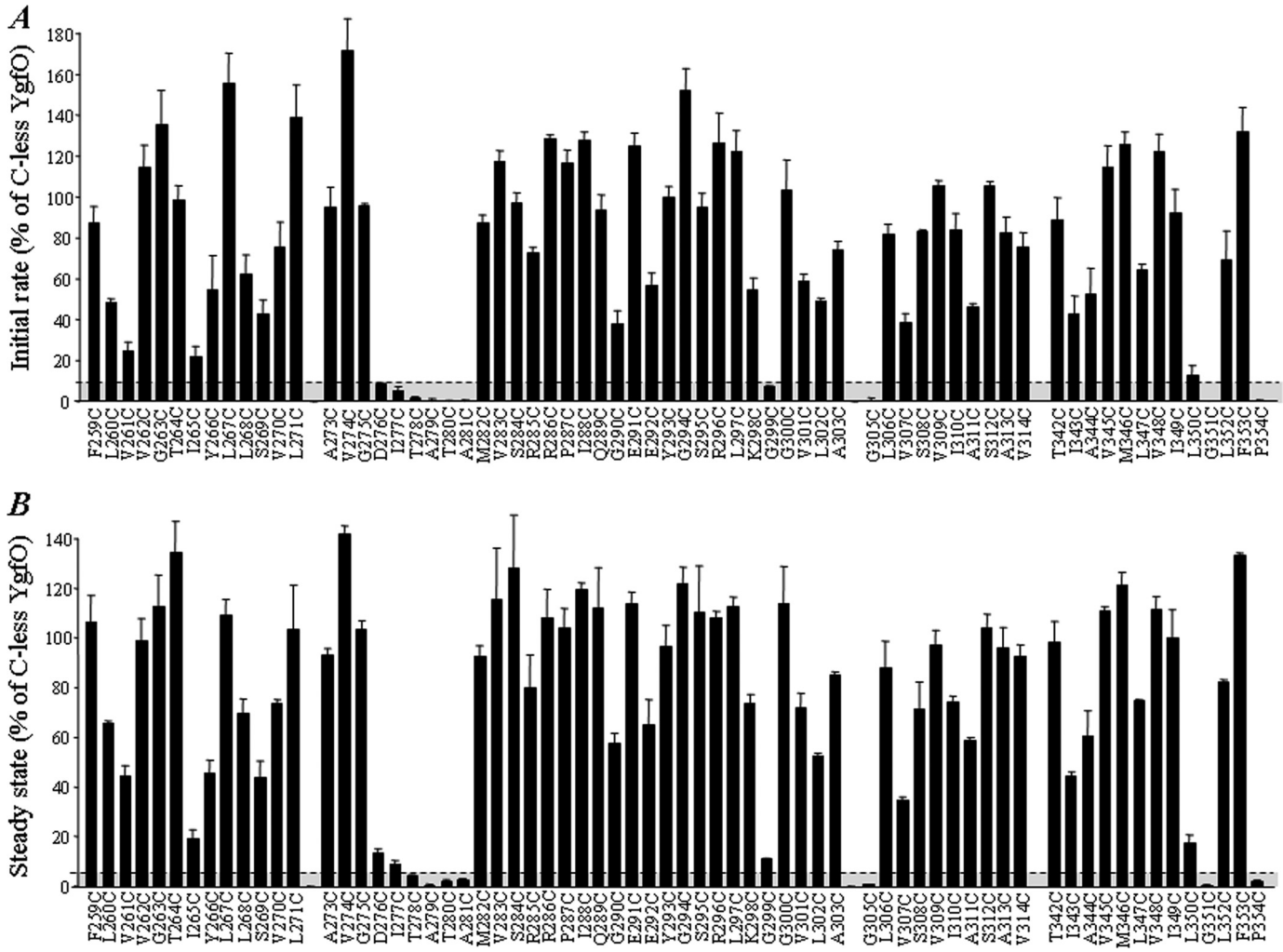

FIGURE 2. **Active xanthine transport activities of single Cys mutants.** *E. coli* T184 harboring pT7-5/*ygfO*(C-less-BAD) with given mutations were grown aerobically at 37 °C in complete medium to mid-logarithmic phase, induced with IPTG (0.5 mM) for 2 h, normalized to 0.7 mg protein per ml of cell suspension, and assayed for transport of [^{3}H]xanthine (1 μM) at 25 °C. *A*, initial rates of uptake measured at 5–20 s. Control values obtained from T184 harboring pT7-5 alone (0.018 nmol mg^{-1} min^{-1} on average) were subtracted from the sample measurements in all cases. Results are expressed as a percentage of the rate of Cys-less YgfO (1.9 nmol mg^{-1} min^{-1} on average) with standard deviations from three independent determinations. *B*, steady state levels of xanthine accumulation (reached at 1–10 min for most mutants). Control values obtained from T184 harboring pT7-5 alone (0.012 nmol mg^{-1} on average) were subtracted from the sample measurements in all cases. Results are expressed as a percentage of the level of Cys-less YgfO (0.8 nmol mg^{-1} on average) with standard deviations from three independent determinations.

tion 276 (Fig. 5). Our data show that all these mutants are expressed to high levels, comparable with those of wild type, but only replacement with Glu (D276E) results in high activity; replacement of Asp-276 with Glu yields xanthine uptake activity that is comparable with wild type, replacement with Asn, Thr, Ala, or Gly yields low but detectable activity (uptake rates and levels of 8–25% relative to wild type), while replacement with His, Gln, Met, Val, or Ile yields inactive mutants (Fig. 5). Kinetic transport analysis shows that mutant D276E displays a K_m approximating wild type and a higher V_{max}, D276N and D276T display wild-type K_m but low V_{max} values, D276A and D276G have impaired affinity (28-fold and 114-fold increased K_m values, respectively), and the remaining mutants display very low or negligible rates of xanthine uptake at any of the concentrations tested, in the range of 0.1 to 100 μM (Table 1). To understand whether extension of the carboxylic side chain of Asp-276 by one methylene group affects the substrate and ligand recognition properties of YgfO, the highly active mutant D276E was assayed for inhibition of [^{3}H]xanthine uptake in the presence or absence of a series of purines and purine analogues (Table 2). It was found that D276E is inefficient to recognize 2-thioxanthine, 3-methylxanthine or 6-thioxanthine, three high-affinity ligands for wild-type YgfO, but displays the novel property to recognize with high affinity 8-methylxanthine (K_i 79 μM) (Table 2 and supplemental Fig. S2).

Replacements of Thr-278, Ala-279, Thr-280, and Ala-281—Residues of the sequence ^{278}TATA^{281} were replaced one by one or in combination with a series of different side chains; Ala residues were replaced with Gly, Ser, Thr, Asn or Val, and Thr residues were replaced with Gly, Ala, Ser, Asn, Gln, or Val (Fig. 6). Our data show that relatively bulky replacements of Ala-279 (A279N, A279V) or Thr-280 (T280N, T280Q, T280V) abolish xanthine uptake activity; two of them (A279V, T280N) abolish expression in the membrane, as well. Replacements of Thr-280 with smaller side chains (T280S, T280A, T280G), replacements of Ala-279 with moderate- or small-volume side chains

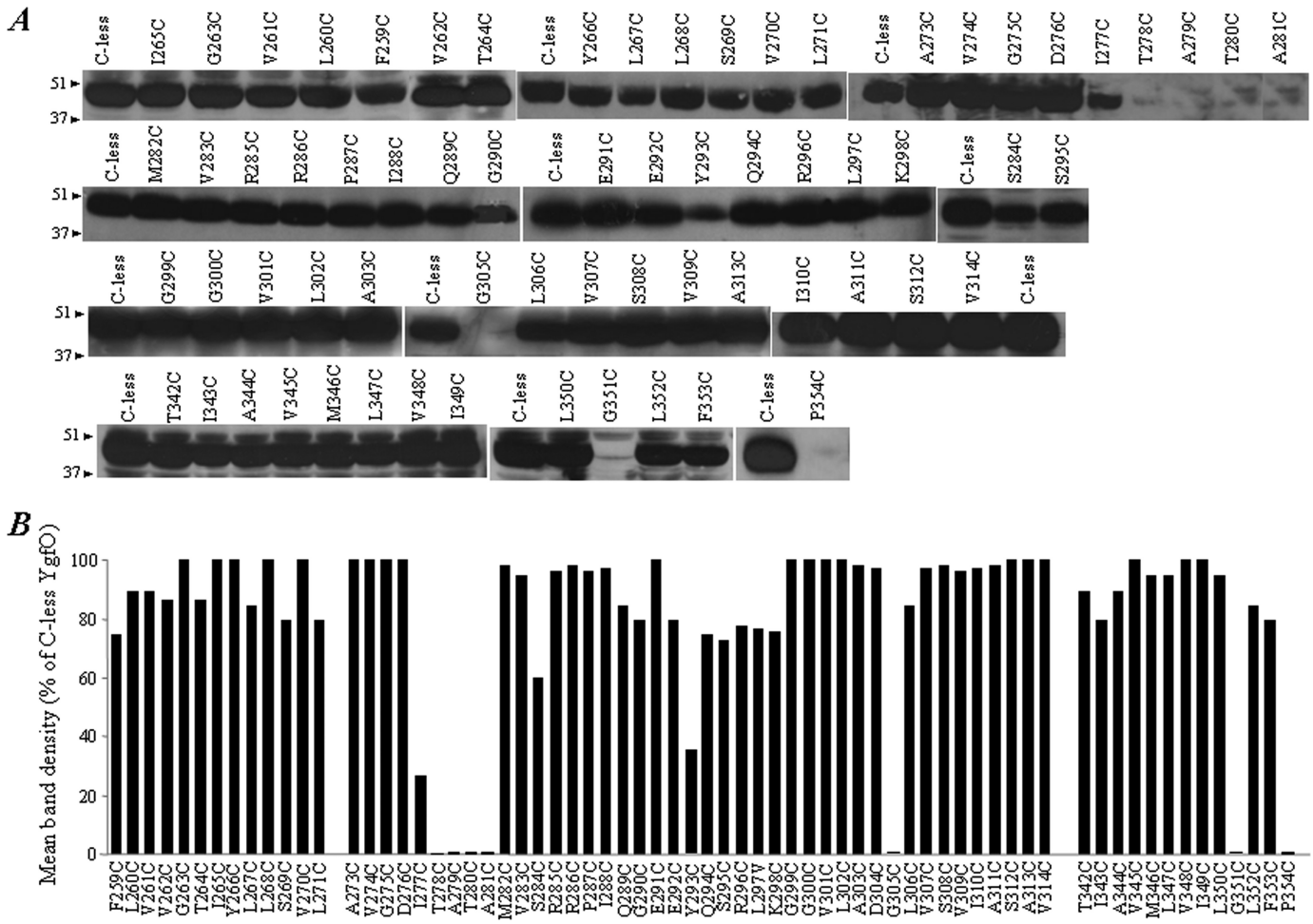

FIGURE 3. **Immunoblot analysis of single Cys mutants.** Membranes were prepared from IPTG-induced cultures of *E. coli* T184 harboring pT7-5/*ygfO*(C-less-BAD) with given mutations. Samples containing ~100 μg of membrane protein were subjected to SDS-PAGE (12%) and immunoblotting using HRP-conjugated avidin. *A*, representative blots of single Cys mutants and Cys-less YgfO. Membranes prepared from cells harboring pT7-5 alone exhibited no immunoreactive material. Prestained molecular mass standards (in kDa; Bio-Rad, low range) are shown on the *left*. *B*, quantitative estimation of the expression level of each mutant as a percentage of Cys-less expression derived from the relative density of the corresponding band, as measured with program Quantity One (Bio-Rad). Results shown are the means of four determinations from two independent experiments, with standard deviations that were <15%.

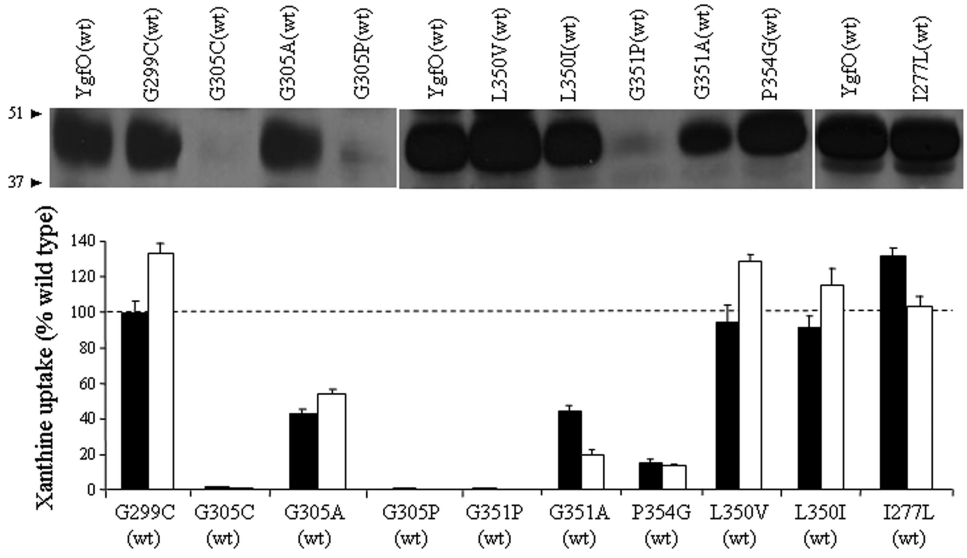

FIGURE 4. **Expression and xanthine uptake activities of site-directed mutants at positions 277, 299, 305, 350, 351, and 354.** *E. coli* T184 harboring pT7-5/*ygfO* (wild-type-BAD) with given mutations were grown, induced and subjected to immunoblot analysis of membrane fractions (*upper panel*) or assayed for transport of [^{3}H]xanthine (1 μM, 25 °C) (*lower panel*), exactly as described in the legends to Figs. 2 and 3. *Open* and *closed histogram bars* represent initial rate and steady-state values, respectively.

(A279T, A279S, A279G) and all studied replacements of Thr-278 or Ala-281 result in relatively high xanthine uptake activity (rates of 40–120% relative to wild type) and expression. Finally, an engineered quadruple mutant of YgfO with modified sequence 278–281 (^{278}ATAT^{281}) was found to display significant expression in the membrane but negligible xanthine uptake activity.

Effect of N-Ethylmaleimide on Transport Activity—The effect of NEM, a membrane-permeable sulfhydryl reagent, on the initial rate of xanthine transport for each active single Cys mutant is presented in Fig. 7. When incubated with 2 mM NEM, it is found that four mutants are inhibited to near completion,

A273C by 89%, V261C by 96%, S284C by 98%, and G275C by 99.5%, an additional four mutants (Y293C, R296C, G300C, V301C) are inhibited by 50–70%, and activity of the remaining 49 single Cys mutants is not altered significantly (<1.5-fold enhancement or inhibition). V261C, A273C, G275C, and S284C were then assayed in the concentration range of 1 μM to 2 mM, and the concentration resulting in half-maximal inhibition (IC_{50}) was determined, in the absence or presence of substrate (xanthine) (Fig. 8). The results show that G275C is highly sensitive to NEM (IC_{50}, 15 μM), while V261C and S284C are moderately sensitive (IC_{50} values, 97 μM and 86 μM) and A273C displays low sensitivity (IC_{50}, 0.98 mM). In the presence of substrate, sensitivity of G275C is enhanced ~2-fold (IC_{50}, 8 μM), while sensitivity of V261C is increased modestly (IC_{50}, 63 μM) and sensitivity of the other mutants is unaffected (Fig. 8).

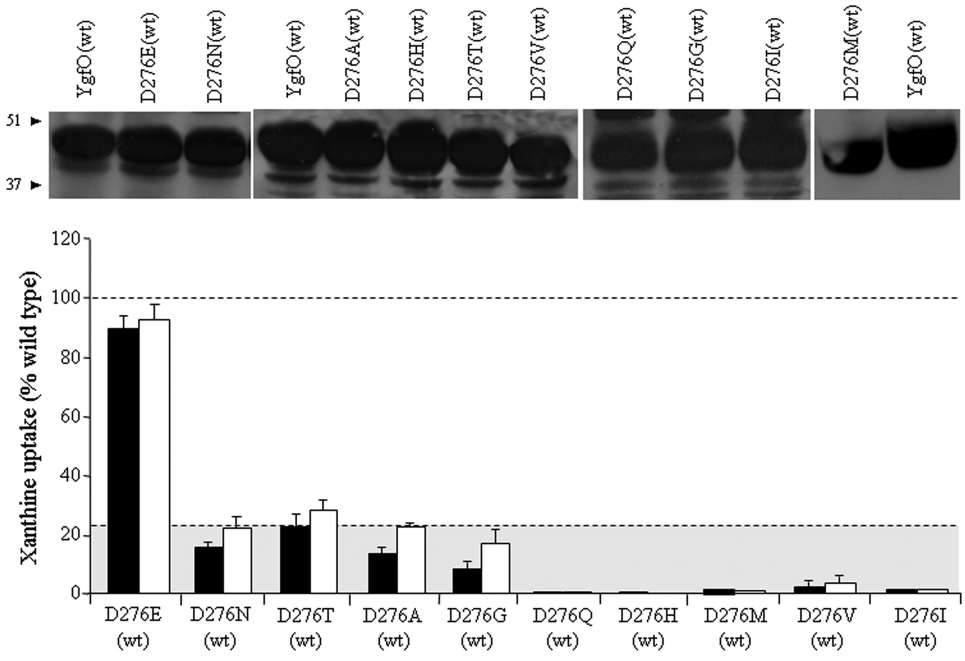

FIGURE 5. **Expression and xanthine uptake activities of site-directed mutants at position 276.** *E. coli* T184 harboring pT7-5/*ygfO*(wild-type-BAD) with given mutations were grown, induced, and assayed exactly as described in the legend to Fig. 4.

DISCUSSION

We have studied the role of amphipathic and putative transmembrane helices flanking the NAT signature motif of YgfO permease and found that important residues cluster in two additional highly conserved motifs, **E**xx**G**-DxxA**T** (TM8) and Gxxx**DG** (TM9a), falling at the approximate cytoplas-

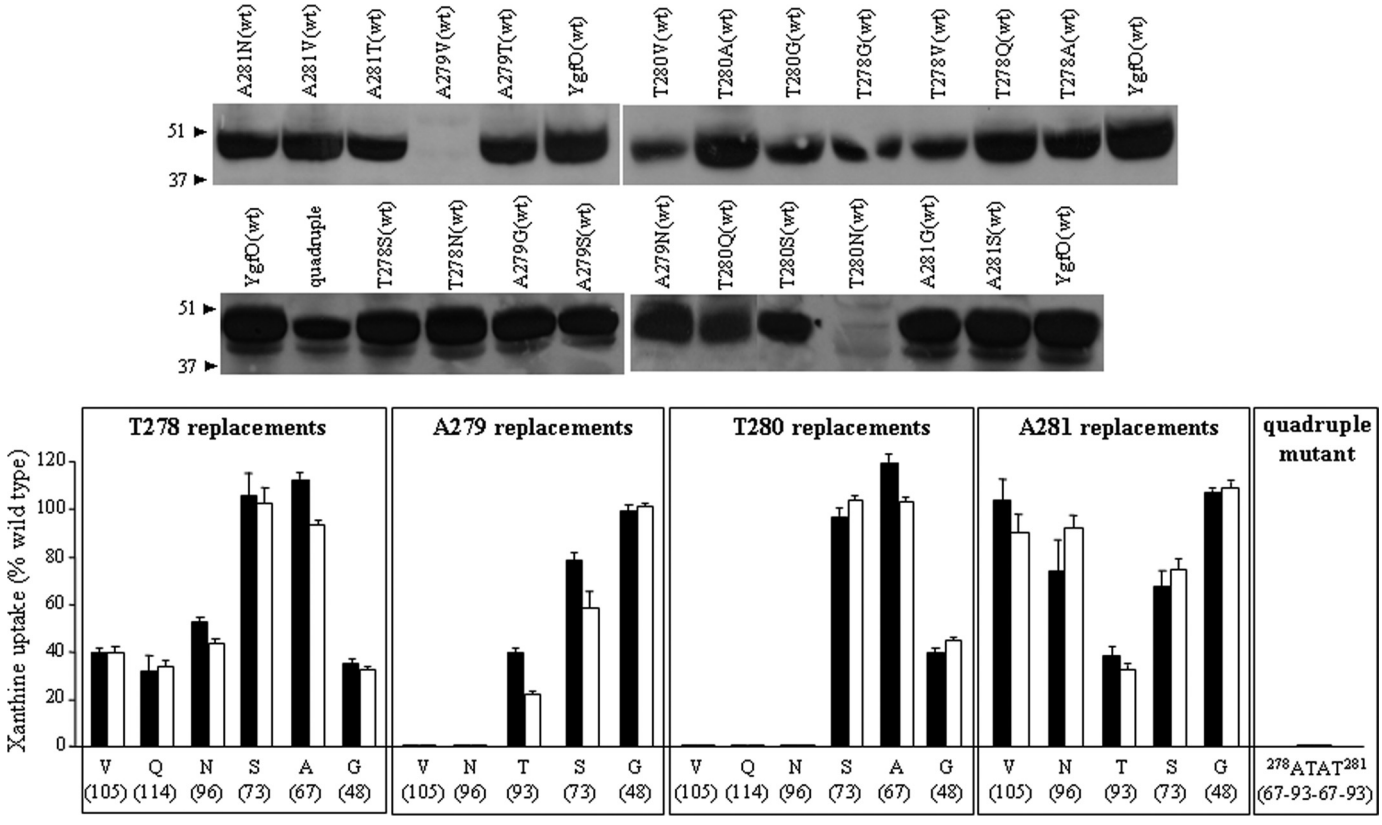

FIGURE 6. **Expression and xanthine uptake activities of site-directed mutants at positions 278, 279, 280, and 281.** *E. coli* T184 harboring pT7-5/*ygfO*(wild-type-BAD) with given mutations were grown, induced, and assayed exactly as described in the legend to Fig. 4. Numbers in *parentheses* shown below each amino acid symbol in the *lower panel* represent van der Waals volumes of the corresponding side chains in Å^3.

TABLE 1

K_m and V_{max} values of YgfO mutants at Asp-276

E. coli T184 expressing the corresponding constructs were assayed for initial rates of xanthine uptake at 5–20 sec, in the concentration range of 0.1–100 μM; negative control values obtained from T184 harboring vector pT7-5 alone were subtracted from the sample measurements in all cases. Kinetic parameters were determined from non-linear regression fitting to the Michaelis-Menten equation using Prism4. Values represent the means of three independent determinations with standard deviations shown. All mutants and the wild-type YgfO version used contained a C-terminal BAD.

Permease	K_m	V_{max}	V_{max}/K_m
	μM	*nmol min^{-1}*	*μl min^{-1} mg^{-1} protein*
YgfO(wt)	4.5 ± 0.5	7.9 ± 1.0	1756
YgfO(C-less)	5.5 ± 0.6	10.2 ± 0.9	1855
D276E(wt)	6.0 ± 0.9	26.3 ± 1.2	4383
D276T(wt)	3.7 ± 1.1	5.5 ± 0.9	1351
D276N(wt)	3.2 ± 0.6	1.9 ± 0.1	594
D276A(wt)	126.8 ± 10.7	36.9 ± 2.4	291
D276G(wt)	516.8 ± 64.6	145.9 ± 17.0	282
D276C(C-less)	17.5 ± 2.7	1.4 ± 0.1	80
D276H(wt)	ND[a]	ND	
D276Q(wt)	ND	ND	
D276M(wt)	ND	ND	
D276V(wt)	ND	ND	
D276I(wt)	ND	ND	

[a] ND, assays were performed, but kinetic values were not determined due to very low uptake rates (≤0.1 nmol mg^{-1} min^{-1}).

TABLE 2

Specificity profile of mutant D276E

E. coli T184 expressing D276E or wild-type YgfO were assayed for initial rates of [^{3}H]xanthine (1 μM) uptake at 5–20 s, in the absence or presence of the indicated unlabeled nucleobases and analogues. For initial assessment of the inhibitory effect, xanthine (1 μM) uptake assays were performed in the presence of a 1000-fold excess (1 mM) of unlabeled competitor and the percentage of the uptake rate retained was determined. The uptake value obtained in the absence of competitor was taken as 100%. Values represent the means of three determinations, with standard deviations <20%. For kinetic inhibition analysis, xanthine (1 μM) transport assays were performed in the presence of 0.001–2 mM of competitor and IC_{50} and K_i values were determined as described under "Experimental Procedures." Most significant differences from the wild-type profile are highlighted in bold. Mutant D276E and the wild-type YgfO version used contained a C-terminal BAD.

	Xanthine uptake rate retained		K_i	
	%	%	μM	μM
Competitor	YgfO(wt)	D276E(wt)	YgfO(wt)	D276E(wt)
Hypoxanthine	91	96	>1000	>1000
Adenine	90	109	>1000	>1000
Guanine	75	88	>1000	>1000
Uracil	98	102	>1000	>1000
6-Thioxanthine	**12**	**61**	**41**	**>1000**
2-Thioxanthine	**15**	**71**	**91**	**>1000**
3-Methylxanthine	**15**	**64**	**72**	**>1000**
8-Methylxanthine	**93**	**11**	**>1000**	**79**
Uric acid	90	100	>1000	>1000
7-Methylxanthine	**100**	**55**	>1000	~1000
Oxypurinol	**30**	**0**	ND[a]	ND
Allopurinol	99	102	>1000	>1000

[a] ND, not determined.

mic loop/helix junctions of TM8 and TM9a (Fig. 1). The first motif includes the functionally irreplaceable Glu-272, which shows a nearly invariable conservation among the members of the NAT/NCS2 family (10), Gly-275, which is absolutely conserved, Asp-276, Thr-278, and Thr-280, which are conserved in the xanthine-transporting homologs, and Ala-279, which is strongly conserved in all known members (supplemental Fig. S1). Important residues in the first half of this motif (Glu-272, Gly-275, Asp-276) form an α-helical face at the cytoplasmic end of TM8 (Fig. 9). The second motif includes the functionally irreplaceable Asp-304, which is conserved as Asp, Asn, or Glu in the known members of the family (10), Gly-305, which is absolutely conserved, as well as the highly conserved Gly-300 (supplemental Fig. S1). Important residues of the second motif (Asp-304, Gly-305) fall on a broad α-helical polar face of TM9a which also includes Ser-308, Ser-312, and Ser-316 (Fig. 9). Overall, our data establish that, in addition to the NAT motif (8, 11) and the two irreplaceable residues of TM8 and TM9a (10), the xanthine permease YgfO contains key determinants at nearby sequence regions, including an essential carboxyl group at Asp-276, constraints in side chain volume and polarity at Ala-279 and Thr-280, sensitivity of Gly-275 (G275C) to site-specific alkylation which is enhanced by substrate, and sensitivity of replacement of Gly-305 to impairment of expression or activity. Two additional residues where replacements lead to very low activity or impaired expression in the membrane cluster in a weaker consensus motif, G*XX*P, at the putative periplasmic end of helix TM9b (Gly-351 and Pro-354) (Fig. 1 and supplemental Fig. S1).

It is clear from our data that optimal activity of YgfO permease requires presence of a carboxyl group at Asp-276. Whereas polar replacements of this residue (Asn, Thr) yield low activity, small non-polar replacements (Gly, Ala) impair affinity for substrate and bulkier hydrophilic or hydrophobic replacements (His, Gln, Met, Val, Ile) result in complete inactivation, replacement of Asp-276 with Glu yields high xanthine uptake activity, which is comparable with wild-type. The high activity of mutant D276E cannot be attributed merely to presence of a negative charge at this position, because alkylation of D276C with negatively charged reagents (2-sulfonatoethyl methanethiosulfonate or iodoacetic acid) does not rescue activity, while restoration of putative intramembrane charge pairing with second-site replacements of mutant D276N (D276N/K164Q or D276N/R385Q) does not lead to increased activity.[5] On the other hand, the extension of the carboxylic side chain of Asp-276 by one methylene group has a profound effect on the ligand recognition properties of YgfO permease, because D276E fails to recognize 2-thioxanthine, 3-methylxanthine, or 6-thioxanthine, three high-affinity ligands for wild-type, but recognizes with high affinity 8-methylxanthine which is not a wild-type ligand (supplemental Fig. S2). This reversal of key specificity elements observed with mutant D276E may be due to different accommodation of substrate in the binding pocket of the permease, associated with the different geometry of the carboxyl group of position 276 with respect to other side chains and/or the purine binding site, and, probably, an altered pK_a for this carboxylate. Consistent with the latter possibility, we find that D276E retains high uptake activity at acidic pH (5.2–6.0), where activity of wild-type is insignificant, and that the ligand profile of D276E is changed at pH 6.0 or lower, restoring in part the wild-type properties (7) (marginal recognition of 8-methylxanthine and high-affinity recognition of 2-thioxanthine and 6-thioxanthine);[5] however, interpretation of this data is complicated, because xanthine itself has a pK_a for monoanion formation of about 7.7 (in solution) (16) and the xanthine substrate of D276E may assume different forms at pH≤6.0 (neutral) and at pH 7.5 (both neutral and anionic). The pleiotropic ligand and pH effects seen with D276E argue against a direct role of this

[5] G. Mermelekas, M. Botou, and S. Frillingos, unpublished observations.

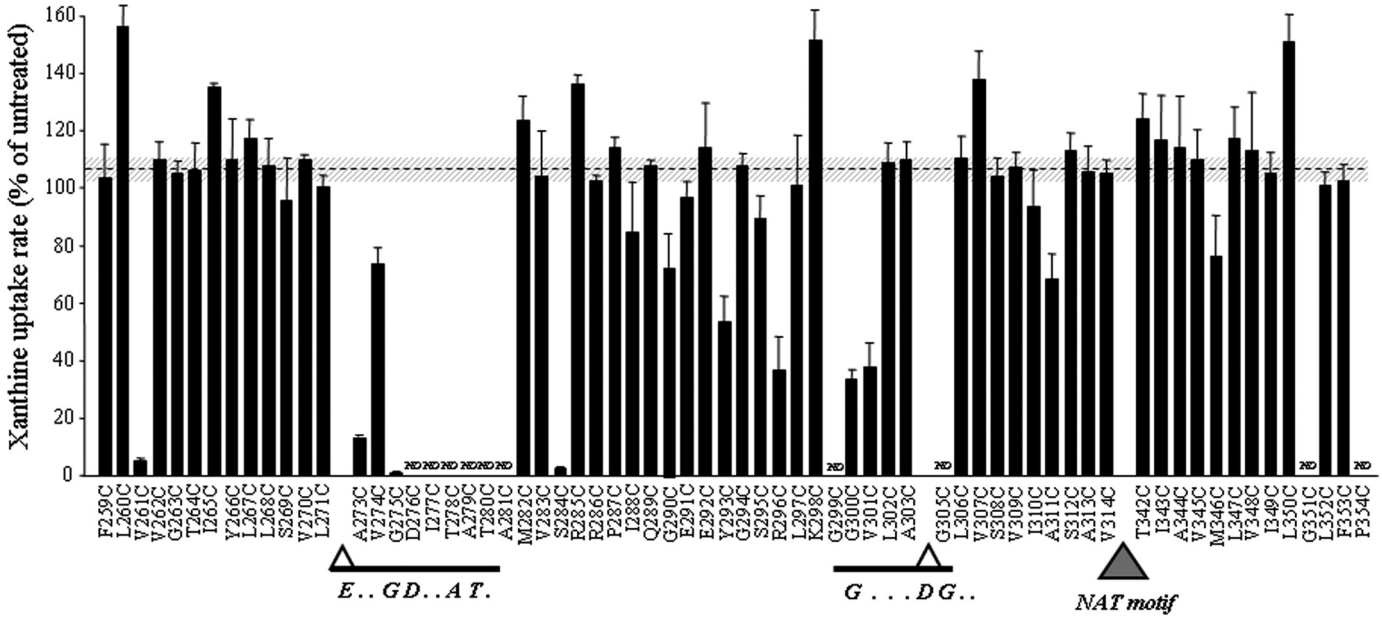

FIGURE 7. **Effect of NEM on the xanthine transport activity of single Cys mutants.** *E. coli* T184 harboring pT7-5/*ygfO*(C-less-BAD) with given mutations were grown, induced, and assayed for transport of [^{3}H]xanthine (1 μM, 25 °C). Cells had been preincubated in the absence or presence of 2 mM NEM for 10 min at 25 °C. Transport assays were performed in the presence of 20 mM potassium ascorbate and 0.2 mM PMS. Rates are presented as percentages of the rate measured in the absence of NEM with standard deviations from three independent determinations shown. Average and standard deviation values of C-less control are also shown as *interrupted line* and *gray horizontal bars*, respectively. Values were not determined (*N.D.*) for mutants D276C, I277C, T278C, A279C, T280C, A281C, G299C, G305C, G351C, or P354C, which display very low or negligible initial rates. Positions of the three conserved sequence motifs **E***XX***G**D*XX***A**T, G*XXX***DG**, and the NAT-signature motif (AQ**N***X***G***XXXX***T**G) are indicated (see also supplemental Fig. S1).

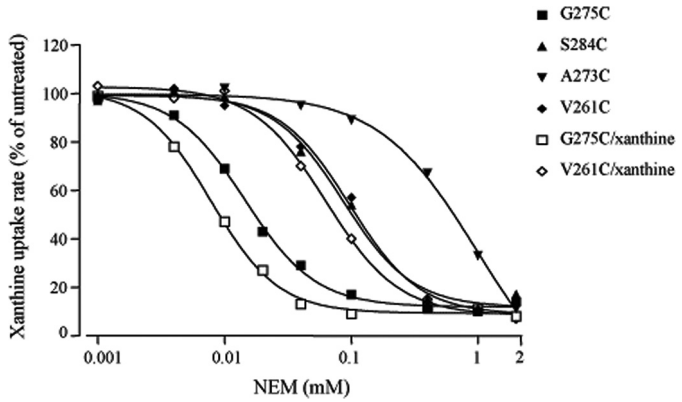

FIGURE 8. **Effect of substrate on the sensitivity of single Cys mutants to inactivation by NEM.** *E. coli* T184 harboring pT7-5/*ygfO*(C-less-BAD) with given mutations were grown, induced, and assayed for transport of [^{3}H]xanthine (1 μM, 25 °C), after preincubation with NEM (0.001–2 mM, 10 min) in the absence or presence of 1 mM xanthine, as indicated. The data shown were fitted to the equation $y = B + (T - B)/(1 + 10^{((\log IC_{50} - \log x)\,h)})$ for sigmoidal dose-response (variable slope), where x is the concentration variable, y (activity) values range from T (*top*) to B (*bottom*) and h is the Hill coefficient, using Prism4, and the IC_{50} values obtained for NEM inhibition were 14.5 μM (G275C), 7.9 μM (G275C/xanthine), 97.2 μM (V261C), 63.0 μM (V261C/xanthine), 86.5 μM (S284C), and 982.3 μM (A273C). Although not shown, IC_{50} values obtained for NEM inhibition of S284C and A273C in the presence of xanthine were identical with the corresponding values obtained in the absence of xanthine.

carboxylate on substrate binding. Similarly, the functionally irreplaceable Glu-272, located one α-helical turn upstream of Asp-276 in putative TM8, does not appear to be essential for high-affinity binding *per se* but, rather, for the conformational changes following binding or coupling purine with proton translocation (10). In addition, single Cys G275C, which falls on the same α-helical face as Glu-272 and Asp-276 (Fig. 9), is highly sensitive to inactivation by NEM and responds to substrate binding with enhanced sensitivity to the reagent, indicating that this α-helical region at the cytoplasmic end of TM8 is conformationally dynamic and substrate binding shifts Gly-275 to a more accessible environment. A similar, but less pronounced, conformational effect is observed with the NEM-sensitive mutant V261C, which falls on the same α-helical face as G275C but disposed toward the periplasmic side of TM8 which is apparently less dynamic (Fig. 9).

Strikingly, a number of relatively bulky replacements or rearrangement of residues in the sequence Thr-Ala-Thr-Ala (278–281) at the end of TM8 (Fig. 1) are incompatible with expression of YgfO in the membrane and/or xanthine uptake activity; the phenomenon is more evident with Ala-279 and Thr-280, for which all bulky replacements tested (side chains of 96–114 Å^3) lead to inactivation and several of them impair expression in the membrane. Replacements that introduce a small change in volume ($\pm$ 6–7 Å^3) but affect the geometry and the polar character of the side chain lead to compromised expression and activity (Ser in place of Ala) or complete loss of expression in the membrane (Cys in place of Thr), whereas replacements of Ala with Thr yield low activity and compromised expression. On the other hand, introduction of side chains that are smaller than the native one by 20–25 Å^3 (Gly in place of Ala, and Ser or Ala in place of Thr) yields wild-type levels of expression and activity, and a most severe decrease (Gly in place of Thr) reduces activity and expression by about 60% (Fig. 6). It is conceivable from these data that Ala-279 and Thr-280, and, to a lesser extent, Thr-278 and Ala-281 may be crucial for packing interactions with helix TM9a (Fig. 1) or another part of the protein, optimizing the permease conformation and/or activity; such interactions of Ala and Thr residues are considered to be very important with respect to helix packing in polytopic membrane

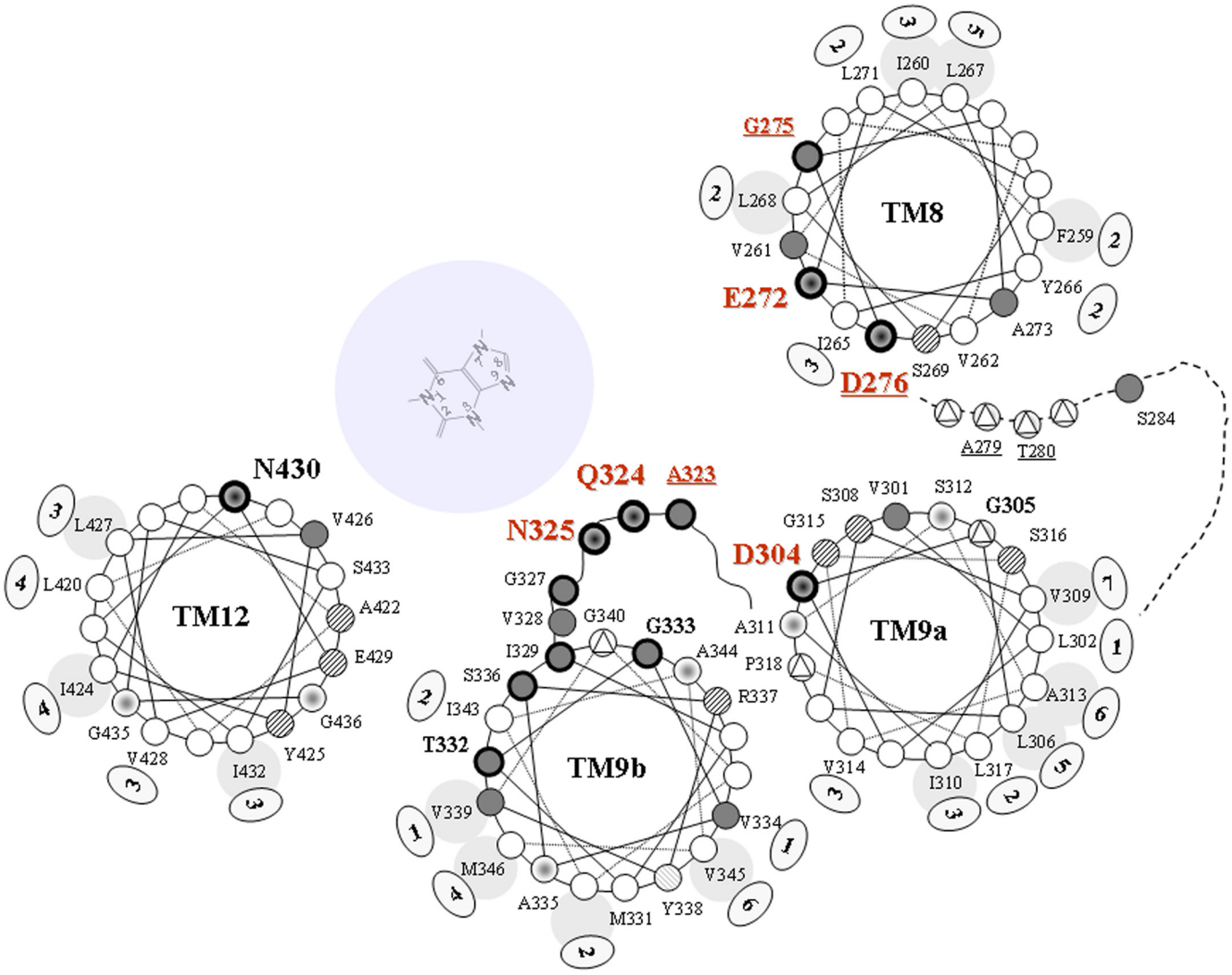

FIGURE 9. **Putative arrangement of TM8, TM9a, TM9b, and TM12 in YgfO permease viewed from the cytoplasmic surface.** Segments of the YgfO sequence are shown as *helical wheel plots* of residues 259–276 (TM8), 301–318 (TM9a), 329–346 (TM9b), and 419–436 (TM12). The four irreplaceable residues (Glu-272, Asp-304, Gln-324, Asn-325) (*red*), Asp-276, which contains an essential carboxyl group (*red*, *underlined*) and Asn-430, which is vicinal to the binding site (9) are *enlarged* and *bolded* and shown as targets. Sites of NEM-sensitive single Cys mutants are shown with a *dark background*, and highly sensitive sites ($IC_{50} \leq 30\ \mu M$) are shown with *bolder peripheries*. Sites which respond to substrate binding by increased sensitivity to inactivation by NEM are indicated in *red* and are *underlined* (Ala-323, Gly-275). Sites where mutants impair expression in the membrane are indicated with a *triangle*. The NAT motif (between TM9a and TM9b) is shown as a re-entrant loop facing the solvent- and substrate-accessible internal cavity (11). Residues conserved either *per se* or with respect to their side chain character in the known members of the family (10) are shown *enlarged*. Sites conserving a hydrophobic side chain in the known members are indicated by a *larger light gray area* facing outside the helix. Sites conserving hydrophobic residues in close sequence homologs of YgfO (sequence identity ≥ 43%) (10) are indicated by an additional *small oval* at the outside of the helix with a *number* denoting the number of different amino acid replacements found at each position. Sites conserving a hydrophilic or a small side chain are shown as *hatched circles* or *targets*, respectively.

proteins (17). It is interesting to note that Thr-280 and, especially, Ala-279 display a high degree of conservation among members of the NAT/NCS2 family (5, 10) and that Ala-363, the residue corresponding to Ala-279 in the fungal homolog UapA (5), has been suggested as critical for function in *Aspergillus nidulans*, based on the loss-of-function phenotype of mutant A363D (18). Although a more comprehensive mutagenesis study of Ala-363 is missing (5, 6), genetic analysis has shown that presence of a Gly in place of Ala-363 is compatible with full UapA activity (18), which is reminiscent of the wild-type expression and activity seen with mutant A279G in YgfO (Fig. 6).

The whole sequence region between TM8 and TM9b has been defined as a domain critical for function and specificity of the fungal UapA (5, 18), based initially on *in vivo* complementation of a set of chimeric transporter constructs in *A. nidulans* (18); this region appears to be involved in dynamic functional interactions with other parts of the protein (TM1, TM12) controlling affinity and specificity for substrate (5). Subsequent studies in both the fungal homolog UapA (4, 5) and the bacterial homolog YgfO (8–11) established that a conserved NAT signature motif within this region (Fig. 1) is essential for substrate recognition and selectivity, and site-directed analysis of YgfO (11) suggested that this motif forms part of the purine binding site (Fig. 9). Our current study addressed systematically for the first time the role of sequences upstream of the NAT motif, and identified another conserved motif (G*XXX***DG**), at the beginning of amphipathic helix TM9a, that is important for YgfO

function, as it contains Asp-304, irreplaceable with respect to active transport (10), and Gly-305, essential for expression in the membrane and optimal activity (Fig. 4); Asp-304 and Gly-305 fall on a broad hydrophilic face of TM9a (Fig. 9) and are flanked by a cluster of four residue positions (Tyr-293, Arg-296, Gly-300, Val-301) which display moderate sensitivity to alkylation with NEM (Fig. 7). Taken together with the finding (10) that Asp-304 is at a conformationally active region not interfering directly with substrate binding, the results imply that the G*XXX***DG** motif is crucial for the interactions and conformational movements associated with the permease turnover. Gly-305, in particular, a residue conserved in all members of the family (3, 10), may confer local flexibility which is needed for turnover and is largely disrupted by replacement with Ala in the low-activity mutant G305A; however, more bulky or rigid replacements (Cys, Pro) appear to disrupt the overall protein folding, leading to abolishment of expression in the membrane. Conformational flexibility of Gly residues has been linked with efficient transport catalysis or substrate binding in other secondary active transporters (19–21). In contrast, the role of Gly-340 (8) and Gly-351 (this study), in helix TM9b of YgfO, may be linked primarily with correct folding and conformational stability of the permease, because all replacements of these Gly residues lead to low or negligible expression in the membrane.

In summary, our findings on TM8, TM9a, and the intervening intracellular loop did not provide any evidence for residues involved directly with substrate binding or specificity, but delineated two dynamic sequence regions which appear to participate in packing interactions and conformational movements that are essential for the permease function. The two sequence regions (**E***XX***G**D*XX***A**T and G*XXX***DG**) form α-helical faces that are probably close together in the tertiary structure of YgfO permease but distal from the purine binding site and the substrate-interacting residues of the NAT motif (Fig. 9). Carboxylic side chains of these sequences (Glu-272, Asp-276, Asp-304) are irreplaceable for YgfO function presumably because they are involved in proton coupling or mechanistically important charge pairs which are affected dramatically by changes in the conformational equilibria of the permease (22); more detailed analysis is needed to elucidate these potential roles, including studies of site-directed alkylation and partial translocation reactions in right-side-out membrane vesicles (22–24), which are in progress in our laboratory. In any event, the roles of these conserved carboxyl groups and, in particular, of Glu-272 and Asp-304, are probably very well conserved in the NAT/NCS2 family, since the corresponding residues of the fungal homolog UapA, Glu-356 and Asp-388, were also delineated as essential for xanthine/uric-acid uptake in a recent random mutagenesis study (5). On the other hand, as revealed from our Cys-scanning analysis (Fig. 1), few or no important residues are encountered in the other regions of the YgfO sequence 257–354 interspacing or flanking the three motifs identified as essential, a finding which further emphasizes the importance of these three motif sequences in TM8 (**E***XX***G**-D*XX***A**T), TM9a (G*XXX***DG**) and the loop between TM9a and TM9b (NAT signature motif, A**QN***X***G***XXXX***T**G).

Acknowledgment—We thank Sotiria Libanovnou for construction and initial analysis of mutants S284C and S296C.

REFERENCES

1. Tsukaguchi, H., Tokui, T., Mackenzie, B., Berger, U. V., Chen, X. Z., Wang, Y., Brubaker, R. F., and Hediger, M. A. (1999) *Nature* **399,** 70–75
2. Yamamoto, S., Inoue, K., Murata, T., Kamigaso, S., Yasujima, T., Maeda, J. Y., Yoshida, Y., Ohta, K. Y., and Yuasa, H. (2010) *J. Biol. Chem.* **285,** 6522–6531
3. Gournas, C., Papageorgiou, I., and Diallinas, G. (2008) *Mol. Biosyst.* **4,** 404–416
4. Koukaki, M., Vlanti, A., Goudela, S., Pantazopoulou, A., Gioule, H., Tournaviti, S., and Diallinas, G. (2005) *J. Mol. Biol.* **350,** 499–513
5. Papageorgiou, I., Gournas, C., Vlanti, A., Amillis, S., Pantazopoulou, A., and Diallinas, G. (2008) *J. Mol. Biol.* **382,** 1121–1135
6. Kosti, V., Papageorgiou, I., and Diallinas, G. (2010) *J. Mol. Biol.* **397,** 1132–1143
7. Karatza, P., and Frillingos, S. (2005) *Mol. Membr. Biol.* **22,** 251–261
8. Karatza, P., Panos, P., Georgopoulou, E., and Frillingos, S. (2006) *J. Biol. Chem.* **281,** 39881–39890
9. Papakostas, K., Georgopoulou, E., and Frillingos, S. (2008) *J. Biol. Chem.* **283,** 13666–13678
10. Karena, E., and Frillingos, S. (2009) *J. Biol. Chem.* **284,** 24257–24268
11. Georgopoulou, E., Mermelekas, G., Karena, E., and Frillingos, S. (2010) *J. Biol. Chem.* **285,** 19422–19433
12. Velho, A. M., and Jarvis, S. M. (2009) *Exp. Cell Res.* **315,** 2312–2321
13. Inoue, H., Nojima, H., and Okayama, H. (1990) *Gene* **96,** 23–28
14. Teather, R. M., Bramhill, J., Riede, I., Wright, J. K., Fürst, M., Aichele, G., Wilhelm, V., and Overath, P. (1980) *Eur. J. Biochem.* **108,** 223–231
15. Granseth, E., Daley, D. O., Rapp, M., Melén, K., and von Heijne, G. (2005) *J. Mol. Biol.* **352,** 489–494
16. Kulikowska, E., Kierdaszuk, B., and Shugar, D. (2004) *Acta Bioch. Pol.* **51,** 493–531
17. Eilers, M., Shekar, S. C., Shieh, T., Smith, S. O., and Fleming, P. J. (2000) *Proc. Natl. Acad. Sci. U.S.A.* **97,** 5796–5801
18. Diallinas, G., Valdez, J., Sophianopoulou, V., Rosa, A., and Scazzocchio, C. (1998) *EMBO J.* **17,** 3827–3837
19. Yernool, D., Boudker, O., Jin, Y., and Gouaux, E. (2004) *Nature* **431,** 811–818
20. Tamura, N., Konishi, S., Iwaki, S., Kimura-Someya, N., Nada, S., and Yamaguchi, A. (2001) *J. Biol. Chem.* **276,** 20330–20339
21. Weinglass, A. B., Smirnova, I. N., and Kaback, H. R. (2001) *Biochemistry* **40,** 769–776
22. Weinglass, A. B., Sondej, M., and Kaback, H. R. (2002) *J. Mol. Biol.* **315,** 561–571
23. Sahin-Tóth, M., Karlin, A., and Kaback, H. R. (2000) *Proc. Natl. Acad. Sci. U.S.A.* **97,** 10729–10732
24. Frillingos, S., and Kaback, H. R. (1996) *Biochemistry* **35,** 10166–10171